Nanoscale Research Letters
a SpringerOpen Journal

NANO EXPRESS Open Access

Nanoscale crystal imperfection-induced characterization changes of manganite nanolayers with various crystallographic textures

Yuan-Chang Liang*, Hua Zhong and Wen-Kai Liao

Abstract

(La,Sr)MnO_3 (LSMO) nanolayers with various crystallographic textures were grown on the sapphire substrate with and without In_2O_3 epitaxial buffering. The LSMO nanolayer with In_2O_3 epitaxial buffering has a (110) preferred orientation. However, the nanolayer without buffering shows a highly (100)-oriented texture. Detailed microstructure analyses show that the LSMO nanolayer with In_2O_3 epitaxial buffering has a high degree of nanoscale disordered regions (such as subgrain boundaries and incoherent heterointerfaces) in the film. These structural inhomogeneities caused a low degree of ferromagnetic ordering in LSMO with In_2O_3 epitaxial buffering, which leads to a lower saturation magnetization value and Curie temperature, and higher coercivity and resistivity.

Keywords: Crystallographic texture; Manganite; Epitaxy; Magnetic properties; Buffering

Background

Because of their versatile physical properties, various transition metal oxides, specifically perovskite-based manganites, have attracted considerable scientific and technological attention [1-3]. There is potential for the application of $La_{1-x}Sr_xMnO_3$ (LSMO) in the magnetic storage device and spin-sensitive device field, or it can be used as an important hole-doping material to construct microelectronic devices [2,4,5]. To realize nanodevice applications with high efficiency, it is imperative that LSMO thin films be fabricated on a nanometric scale.

High-quality epitaxial manganite films with specific orientations are essential for the next-generation of microelectronic and magnetic devices. However, single-crystalline perovskite oxide substrates are expensive, and a large diameter substrate is currently technologically unavailable. These factors hinder the practical application of epitaxial LSMO films in the electronic industry [4,6]. Two factors might cause lattice stress in nanoscale manganite thin films. An ultra-thin LSMO epilayer grown on the lattice-mismatched perovskite oxide substrate usually induces built-in stresses in the film, which greatly affect its physical properties [4,7-9]. Moreover, a large thermal expansion coefficient (TEC) difference between the film and substrate also significantly affects the lattice stress in nanoscale manganite thin films. In comparison to randomly oriented thin films, the highly crystallographic textured film usually exhibits superior crystal quality. If the TEC value of a substrate and film is similar, then highly textured ultra-thin polycrystalline LSMO films would not suffer from the lattice distortion that was caused by a lattice mismatch on the single crystalline substrates. This might be promising for practical applications in devices. The sapphire substrate and LSMO have similar TEC sizes [10]. Sapphire substrates can be fabricated with a large diameter and relatively low cost in comparison to perovskite oxide substrates. Such fabrication could attain the practical mass production of a device. Moreover, to form functional heterostructure microelectronic devices, sapphire substrates can be used to integrate LSMO nanofilms with other high-quality optoelectronic thin films [11,12]. During this project, two different crystallographic textured LSMO thin films with a nanoscale thickness were grown using In_2O_3 epitaxial underlayering. These films did not suffer lattice stress. These results enable an analysis of the correlation between nanoscale crystal imperfections and manganite nanofilm physical properties.

* Correspondence: yuanvictory@gmail.com
Institute of Materials Engineering, National Taiwan Ocean University, Keelung 20224, Taiwan

Methods

LSMO nanolayers (the Sr content is approximately 39%) with thickness of approximately 60 nm were grown on the *c*-axis-oriented sapphire substrates with and without 40-nm-thick In_2O_3 (222) epitaxial buffering. The deposition of the In_2O_3 epitaxy layers and LSMO nanolayers was performed using a radiofrequency magnetron-sputtering system. During the deposition, the substrate temperature for the thin-film growth of the In_2O_3 epitaxy and LSMO nanolayer was kept at 600°C and 750°C, respectively. Moreover, the gas pressure of deposition was fixed at 10 mTorr with an Ar/O_2 ratio of 3:1. The as-synthesized samples are further annealed in air ambient at 950°C for 30 min.

The crystal structure of the samples was investigated by X-ray diffraction (XRD) with Cu Kα radiation. The detailed microstructure of the as-synthesized samples was characterized by scanning electron microscopy (SEM) and high-resolution transmission electron microscopy (HRTEM). The composition analysis was performed using energy dispersive X-ray spectrometer (EDS) attached to the TEM. The surface morphology of the LSMO nanolayers was investigated by atomic force microscopy (AFM) with an area size of 2 μm × 2 μm. The surface current images of the LSMO nanolayers were also observed using conductive atomic force microscopy (CAFM) with PtIr tips. A superconducting quantum interference device magnetometer was used to measure the magnetic properties of the samples.

Results and discussion

Figure 1a,b shows the XRD patterns of the LSMO nanolayers grown on sapphire substrates with and without In_2O_3 epitaxial buffering, respectively. In addition to Bragg reflection from the In_2O_3 (222) and Al_2O_3 (0001) crystallographic planes, clear Bragg reflections of (100), (110), and (200) were present for the pseudo-cubic LSMO in the XRD measurement range. The XRD results show a highly (110)-oriented crystallographic feature of the LSMO nanolayer grown on the In_2O_3 (222) epitaxy. By contrast, a highly (*h*00)-oriented crystallographic feature was observed for the LSMO nanolayer grown on the bare sapphire substrate. The LSMO nanolayers with and without In_2O_3 epitaxial buffering are in a pseudocubic structure with a similar lattice constant of 0.387 nm. This is similar to the bulk value [4], demonstrating that no lattice distortion exists in the nanofilms. Interplanar spacing, corresponding to (110) LSMO plane (0.276 nm), is more similar to (222) plane of the In_2O_3 (0.292 nm) in comparison to the (100) LSMO plane. Moreover, a large lattice mismatch (approximately −13.2%) exists between In_2O_3 (222) and sapphire (0001) [13]. This information suggests that LSMO (110) growth on In_2O_3 (222) has a higher crystallographic compatibility degree during *in situ* crystal growth. Figure 1c,d shows the LSMO nanolayer SEM images with and without In_2O_3 epitaxial buffering, respectively. The grains are densely compacted, and no pores are found in the film surfaces. Furthermore, the grain size is more homogeneous for the LSMO nanolayers grown on the sapphire substrate. The LSMO grain sizes range from approximately 50 to 80 nm for the LSMO nanolayers on the sapphire substrate. The grains lying on the In_2O_3 epitaxially buffered sapphire substrate range from approximately 50 to 120 nm in size.

Figure 2a shows the cross-sectional TEM morphology of the LSMO nanolayer with In_2O_3 epitaxial buffering.

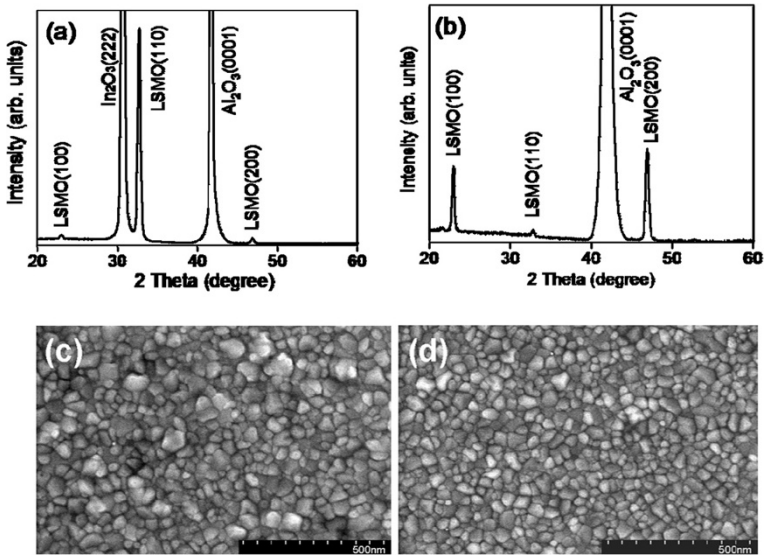

Figure 1 XRD patterns and SEM images of LSMO nanolayer with and without In_2O_3 epitaxial buffering. XRD patterns of LSMO nanolayer **(a)** with and **(b)** without In_2O_3 epitaxial buffering. SEM images of LSMO nanolayer **(c)** with and **(d)** without In_2O_3 epitaxial buffering.

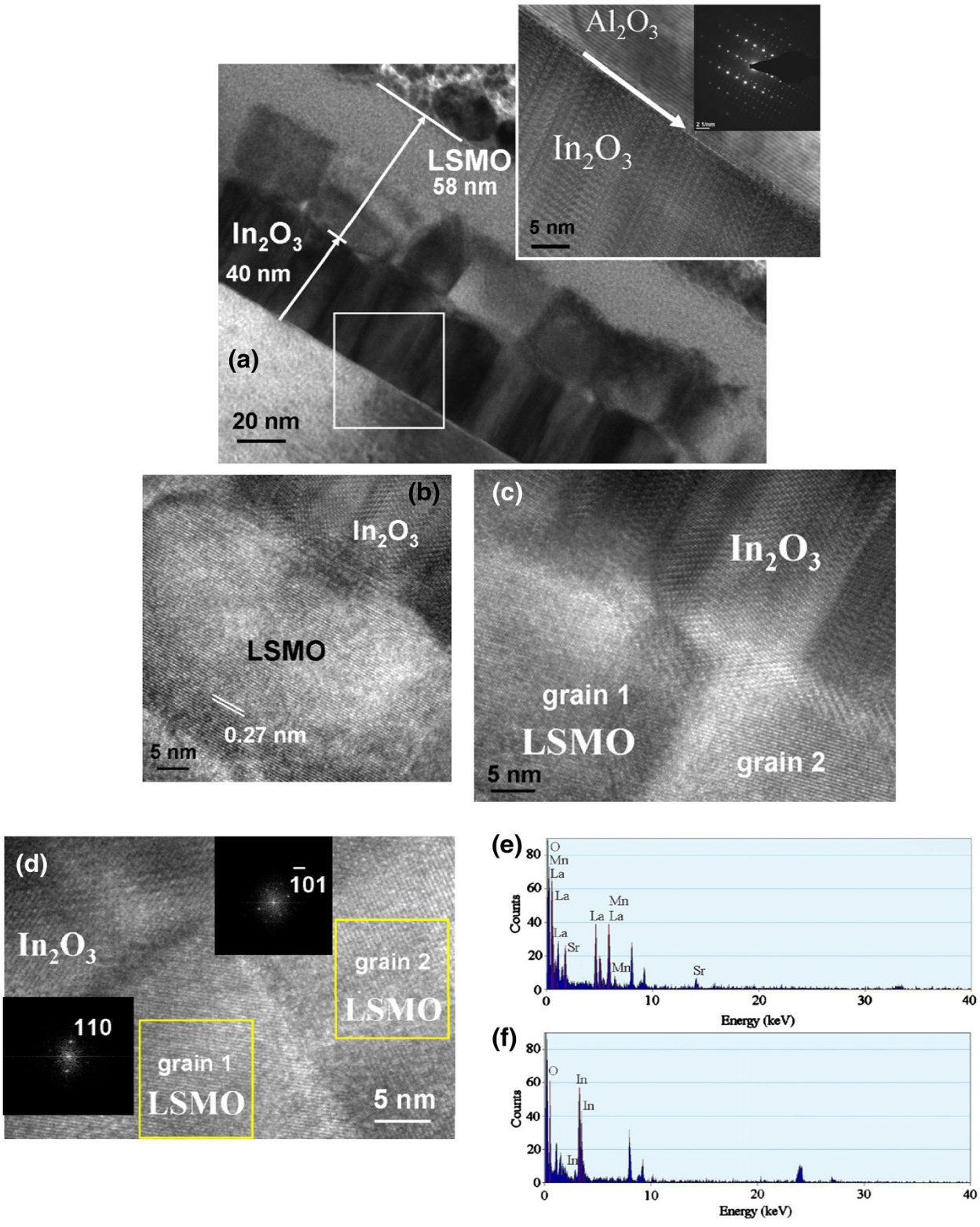

Figure 2 (See legend on next page.)

(See figure on previous page.)
Figure 2 TEM and HRTEM images and EDS spectra of LSMO nanolayer and In_2O_3 epitaxy. (a) Low-magnification TEM image of the LSMO nanolayer with In_2O_3 epitaxial buffering on the sapphire substrate. The HRTEM image was taken from the interface of the In_2O_3epitxay-sapphire substrate (white square region), and the inset shows the corresponding electron diffraction pattern at the heterointerface. **(b)** HRTEM image taken from the local single LSMO nanograin on the In_2O_3 epitaxy. **(c**, **d)** HRTEM images taken from the different local regions containing two neighboring LSMO nanograins on the In_2O_3 epitaxy. The corresponding FFT patterns taken from the different oriented LSMO nanograins are also shown in the insets of **(d)**. **(e)** EDS spectrum taken from the LSMO nanolayer. **(f)** EDS spectrum taken from the In_2O_3 epitaxy.

The In_2O_3 epitaxy has approximately a 40-nm thickness and exhibits a columnar crystallite feature. The inset shows the In_2O_3 epitaxial high-resolution (HR) lattice fringes on the sapphire substrate. A clear interface was formed between the film and the substrate. The electron diffraction pattern taken from the interface of the In_2O_3 film and sapphire substrate also confirms that the In_2O_3 (222) epitaxial layer was grown on the *c*-axis-oriented sapphire substrate [11]. Moreover, a bilayer feature was observed on the LSMO nanolayer (Figure 2a). The total thickness of the LSMO nanolayer is approximately 58 nm, with a thinner 23-nm-thick homogeneous top sublayer, which is formed because of poor thin-film protection during the TEM sample preparation by focused ion beam milling. This may have caused a thermal effect and/or beam damage on the upper side of LSMO nanolayer. However, the lower side of the LSMO nanolayer maintained well crystalline granular features. The LSMO grains nucleated from the rugged surface of the columnar In_2O_3 epitaxy during thin-film growth. This caused the heterointerface between the LSMO nanolayer and In_2O_3 epitaxy to be rugged. Further investigation of the HR lattice fringes of one LSMO grain (Figure 2b) revealed that the interplanar d-spacing is approximately 0.276 nm in correspondence to the {110} lattice arrangement. A mechanism that matches the local domain epitaxy under a proper thin-film growth process demonstrated that it can form single-crystal LSMO grains with specific orientations [14]. Figure 2c,d shows the HR lattice fringes of the granular LSMO film taken from the different regions adjacent to the In_2O_3 epitaxy. A thin layer (approximately 2 nm in thickness marked with red boundaries) that serves as a transition boundary was formed between the LSMO nanograins and In_2O_3 epitaxy (Figure 2c). A similar crystallographic disorder, with an approximately 2-nm thickness, between the film and underlayer was shown in the perovskite LSMO and $SrTiO_3$ epilayers grown on lattice mismatched materials [15]. This crystallographic disorder region is associated with a lattice strain relief between the film and the underlayer. The fast Fourier transformation (FFT) patterns in Figure 2d shows two misoriented nanograins. Depending on the relative rotation among the different grains during thin-film growth, the subgrain boundaries are formed among the nanograins. The TEM image shows that the subgrain boundaries on the nanometric scale combine the discrete-oriented crystallites to form a continuous LSMO nanolayer. Quantization of the spectrum in Figure 2e shows that the contents of La, Sr, Mn, and O are approximately 12.45, 7.85, 22.11, and 57.59 at %, respectively, for the LSMO thin layer. Therefore, approximately 38.7 at % of Sr dopant was achieved within the LSMO. Figure 2f exhibits that the element contents of the In_2O_3 layer are slightly oxygen deficient (the contents of In and O are approximately 46.19 and 53.81 at %, respectively). This is because the In_2O_3 epitaxy was grown under an oxygen-deficient atmosphere.

Figure 3a shows the cross-sectional TEM morphology of the LSMO nanolayer grown on the bare sapphire substrate. A similarly damaged thin-layer was observed herein. Notably, granular LSMO layer contrast changes suggest that the film is composed of different LSMO crystallite orientations. Comparatively, the LSMO on the sapphire substrate experienced a relatively small degree of contrast changes, which cause the film structure to be more homogeneous than that on the In_2O_3 epitaxy. The insets show HR lattice fringes taken from different local regions at the interfaces between the LSMO nanograins and the sapphire substrate. Two types of heterointerface between the LSMO and substrate were presented. In the left inset, a thin (approximately 2 nm thick) transition layer formed at the heterointerface. By contrast, the right inset exhibits a high degree of interface coherency between the LSMO nanograin and substrate. The observation demonstrated that local single-crystal LSMO grains can be formed on the sapphire substrate with a sharp heterointerface during thin-film growth. The heterointerface between the LSMO nanolayer and the sapphire substrate is relatively flat and smooth in comparison to the one grown on the In_2O_3 epitaxy. This is believed to reduce the potential crystal defects at the heterointerface. Moreover, the FFT patterns and HR lattice fringes revealed that a thin disordered region was formed between the misoriented nanograins (Figure 3b).

Figure 4a,b shows the surface topography of LSMO nanolayers with and without In_2O_3 epitaxial buffering. Comparatively, with a root-mean-square (rms) roughness of 1.7 nm, the surface of the LSMO nanolayer grown on the bare sapphire substrate was smoother. The rms surface roughness of the film with In_2O_3 epitaxial buffering is 3.5 nm. As observed from the SEM images, the roughening of the LSMO nanolayer surface grown on the In_2O_3 epitaxy might be associated with its irregular grain sizes. Figure 4c,

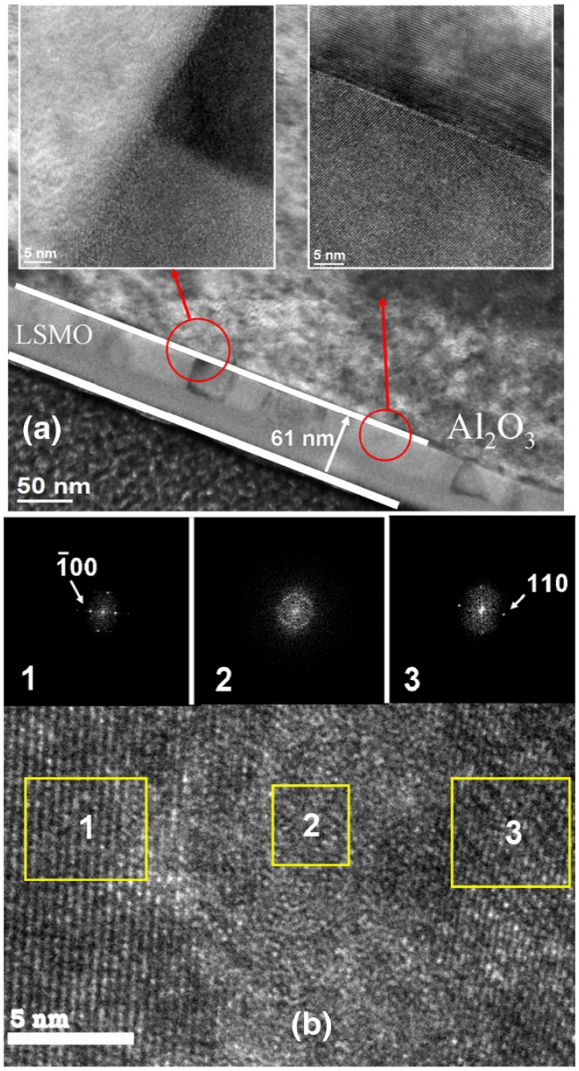

Figure 3 Cross-sectional TEM morphology of the LSMO nanolayer, FFT patterns, and HR lattice fringes. (a) Low-magnification TEM image of the LSMO nanolayer on the sapphire substrate. The insets show the HRTEM images of LSMO nanolayer on the sapphire with (right) and without (left) sharp interface. **(b)** HRTEM image taken from the local regions containing different oriented LSMO nanograins. The corresponding FFT patterns taken from regions 1, 2, and 3 are also shown.

d shows the spatial distributions of currents at the micro- and/or nano-scale of the LSMO nanolayers with and without In_2O_3 epitaxy measured at a fixed applied bias during AFM scanning. The LSMO nanolayer current maps show that the dark regions only account for a remarkably small ratio over the area of interest, revealing that the LSMO nanolayer surfaces remain a conductive characteristic under 0.05V. In comparison, the LSMO nanolayer without In_2O_3 epitaxial buffering has a homogeneously spatial distribution of current spots over the measured area. The current mean statistic value distributed over the measured area is 30.3 and 38.8 pA for the LSMO nanolayers with and without In_2O_3 epitaxial buffering, respectively. The LSMO nanolayer with In_2O_3 epitaxial buffering is slightly more resistant than the film without buffering.

Figure 5a,b shows the magnetization vs. temperature curves (*M-T*) for the zero-field-cooled (ZFC) and field-cooled (FC) samples. The applied magnetic field was 1,000 Oe during the *M-T* measurements. The *M-T* curves demonstrated that the LSMO nanolayers have a sharp ferromagnetic to paramagnetic transition. Comparatively, a higher magnetization and Curie temperature was observed for the LSMO nanolayers without In_2O_3 epitaxial buffering. The Curie temperatures of the LSMO nanolayers with and without In_2O_3 epitaxial buffering were 290 and 323K, respectively. A higher ferromagnetic ordering degree causes the LSMO films to have a higher saturation magnetization value and Curie temperature [16]. This reveals that more structural inhomogeneities in the LSMO nanolayer with In_2O_3 epitaxial buffering caused the double-exchange mechanism to have a greater depression degree [17]. Moreover, the higher moment in manganite thin films was attributed to a lower resistivity of the film [18]. This is in agreement with the CAFM measurements that convey that the LSMO nanolayer with In_2O_3 epitaxial buffering is slightly more resistant than the film without buffering. There is a large difference in the ZFC and FC curves' low temperature range. ZFC curves display a broad summit peak. A larger difference in magnetization between the ZFC and FC curves in the low temperature region was observed for the LSMO nanolayer with In_2O_3 epitaxial buffering, which conveyed that randomly oriented magnetic domains are more difficult to align in the film. The subgrain boundaries among the LSMO nanograins, rough film surfaces, and interfaces caused an existence of disordered spins in the LSMO nanolayer. These disordered spins might play an important role in separating the magnetically ordered regions in the LSMO nanolayer [19]. This caused the marked cluster glass state in the film. Figure 5c,d shows the magnetization-field (*M-H*) hysteresis curves at 50 K for LSMO nanolayers with and without In_2O_3 epitaxial buffering. The field was applied parallel to the substrates. The respective in-plane saturated magnetization value was approximately 500 and 625 emu/cm^3 for the LSMO nanolayers with and without In_2O_3 epitaxial buffering, respectively. The LSMO nanolayers with and without In_2O_3 epitaxial buffering have coercive fields that are 90 and 72 Oe, respectively. The crystal imperfections, such as surface roughness, subgrain boundary, and heterointerface, play important roles in determining the coercivity [7]. Several results conveyed that the surface roughness provides an extra hindrance to the magnetization reversal and induces an increase in coercivity accordingly [20]. Moreover, a

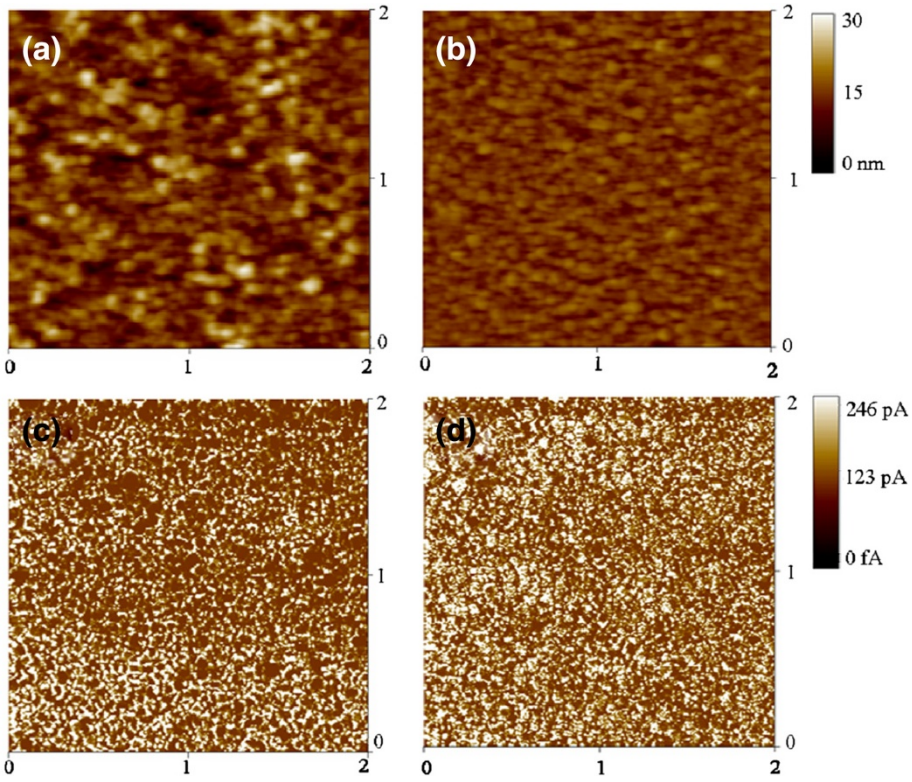

Figure 4 AFM and CAFM images of the LSMO nanolayer. AFM images of the LSMO nanolayer **(a)** with and **(b)** without In_2O_3 epitaxial buffering. CAFM images of the LSMO nanolayer **(c)** with and **(d)** without In_2O_3 epitaxial buffering.

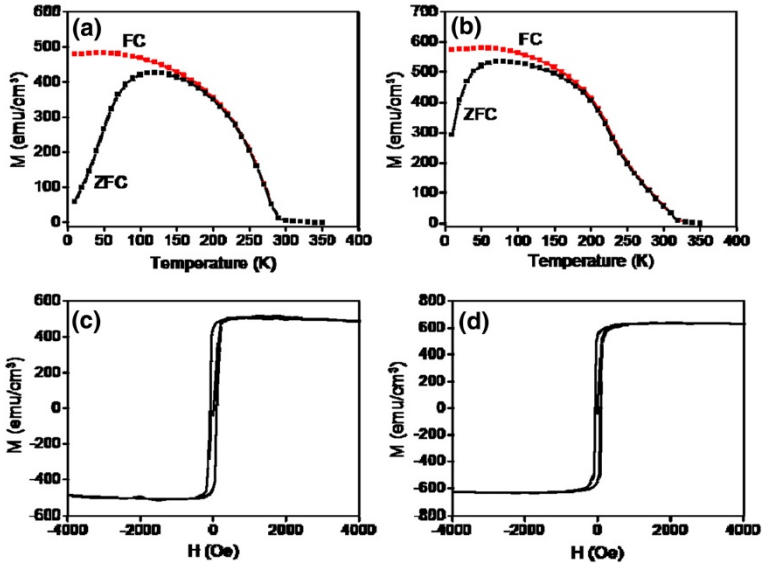

Figure 5 FC and ZFC *M-T* curves. Field-cooled and zero-field-cooled *M-T* curves of the LSMO nanolayer **(a)** with and **(b)** without In_2O_3 epitaxial buffering. *M-H* curve of the LSMO nanolayer **(c)** with and **(d)** without In_2O_3 epitaxial buffering.

greater degree of structural inhomogeneities (rugged heterointerfaces and subgrain boundaries) in the LSMO nanolayer with In_2O_3 epitaxial buffering act as domain-wall pinning centers [17]. The relatively low coercivity is attributed to the high quality, low defect density of the LSMO nanolayer without buffering. The structural analyses support the observed *M-H* results.

Conclusions

In summary, 60-nm-thick LSMO nanolayers were grown on sapphire substrates with and without In_2O_3 (222) epitaxial buffering. The LSMO experienced improved (110) preferred crystal growth via In_2O_3 (222) epitaxial buffering. Comparatively, the surface grain size is more homogeneous for the LSMO nanolayer grown on the sapphire substrate. The rugged surface of the In_2O_3 epitaxial underlayer further incurred rougher surface morphology of the LSMO nanofilm. The columnar crystallite feature of the In_2O_3 epitaxial underlayer caused a relatively smaller lateral domain size of the manganite ultra-thin layer on it. Moreover, In_2O_3 epitaxial buffering resulted in rugged heterointerfaces between the LSMO nanolayer and In_2O_3 epitaxy. These factors contributed to a higher content of subgrain boundaries and incoherent interfaces on a nanometric scale in the LSMO nanofilm via In_2O_3 epitaxial buffering. These disordered regions caused disordered spins to exist in the LSMO nanolayer. Therefore, lower saturation magnetization value and Curie temperature, and higher coercivity and resistivity are found in the highly (110)-textured LSMO nanolayer.

Competing interest

The authors declare that they have no competing interests.

Authors' contributions

YCL designed the experiments and drafted the manuscript. HZ carried out the thin-film preparation and material analyses. WKL analyzed the AFM and CAFM data. All authors read and approved the final manuscript.

Authors' information

YCL is a professor of the Institute of Materials Engineering at National Taiwan Ocean University (Taiwan). HZ received his Masters degree in Materials Engineering at National Taiwan Ocean University (Taiwan) in 2013. WKL is a graduate student of the Institute of Materials Engineering at National Taiwan Ocean University (Taiwan).

Acknowledgments

This work is supported by the National Science Council of Taiwan (grant nos.: NSC102-2221-E-019-006-MY3 and NSC100-2628-E-019-003-MY2) and National Taiwan Ocean University (grant no.: NTOU-RD-AA-2012-104012).

Received: 9 May 2013 Accepted: 6 July 2013
Published: 6 August 2013

References

1. Liang YC, Liang YC: **Correlation between lattice modulation and physical properties of $La_{0.72}Ca_{0.28}MnO_3$ films grown on $LaAlO_3$ substrates.** *J Crystal Growth* 2007, **303:**638–644.
2. Sahu DR: **Lateral parameter variations on the properties of $La_{0.7}Sr_{0.3}MnO_3$ films prepared on Si (1 0 0) substrates by dc magnetron sputtering.** *J Alloys Compounds* 2010, **503:**163–169.
3. Tsuchiya T, Daoudi K, Manabe T, Yamaguchi I, Kumagai T: **Preparation of the $La_{0.8}Sr_{0.2}MnO_3$ films on STO and LAO substrates by excimer laser-assisted metal organic deposition using the KrF laser.** *Appl Surf Sci* 2007, **253:**6504–6507.
4. Liang YC, Liang YC: **Strain-dependent surface evolution and magneto-transport properties of $La_{0.7}Sr_{0.3}MnO_3$ epilayers on $SrTiO_3$ substrates.** *J Crystal Growth* 2007, **304:**275–280.
5. Liang YC, Hu CY, Zhong H, Wang JL: **Crystal synthesis and effects of epitaxial perovskite manganite underlayer conditions on characteristics of ZnO nanostructured heterostructures.** *Nanoscale* 2013, **5:**2346–2351.
6. Yang Z, Sun L, Ke C, Chen X, Zhu W, Tan O: **Growth and structure properties of $La_{1-x}Sr_xMnO_{3-\sigma}$ (x = 0.2, 0.3, 0.45) thin film grown on $SrTiO_3$ (0 0 1) single-crystal substrate by laser molecular beam epitaxy.** *J Crystal Growth* 2009, **311:**3289–3294.
7. Du YS, Wang B, Li T, Yu CB, Yan H: **Effects of annealing procedures on the structural and magnetic properties of epitaxial $La_{0.7}Sr_{0.3}MnO_3$ films.** *J Mag Mag Mater* 2006, **297:**88–92.
8. Vailionis A, Boschker H, Siemons W, Houwman EP, Blank DHA, Rijnders G, Koster G: **Misfit strain accommodation in epitaxial ABO3 perovskites: lattice rotations and lattice modulations.** *Phys Rev B* 2011, **83:**064101–064111.
9. Lee YH, Lee CC, Liu ZX, Liang CS, Wu JM: **Epitaxial growth of the La-substituted $BiFeO_3$ thin films.** *Electrochem Solid State Lett* 2006, **9:**F38–F40.
10. Choi KK, Taniyama T, Yamazaki Y: **Strain-induced anisotropic low-field magnetoresistance of La–Sr–Mn–O thin films.** *J Appl Phys* 2001, **90:**6145–6151.
11. Liang YC, Lee HY: **Growth of epitaxial zirconium-doped indium oxide (222) at low temperature by rf sputtering.** *Cryst Eng Comm* 2010, **12:**3172–3176.
12. Dai J, Liu H, Fang W, Wang L, Pu Y, Jiang F: **Comparisons of structural and optical properties of ZnO films grown on (0 0 0 1) sapphire and GaN/(0 0 0 1) sapphire template by atmospheric-pressure MOCVD.** *Mat Sci Eng* 2006, **B127:**280–284.
13. Mei ZX, Wang Y, Du XL, Zeng ZQ, Ying MJ, Zheng H, Jia JF, Xue QK, Zhang Z: **Growth of In_2O_3 single-crystalline film on sapphire (0 0 0 1) substrate by molecular beam epitaxy.** *J Crystal Growth* 2006, **289:**686–689.
14. Narayan J, Larson BC: **Domain epitaxy: a unified paradigm for thin film growth.** *J Appl Phys* 2003, **93:**278–285.
15. Pradhan AK, Hunter D, Williams T, Lasley-Hunter B, Bah R, Mustafa H, Rakhimov R, Zhang J, Sellmyer DJ, Carpenter EE, Sahu DR, Huang JL: **Magnetic properties of $La_{0.6}Sr_{0.4}MnO_3$ thin films on $SrTiO_3$ and buffered Si substrates with varying thickness.** *J Appl Phys* 2008, **103:**023914–023922.
16. Ju HL, Gopalakrishnan J, Peng JL, Li Q, Xiong GC, Venkatesan T, Greene RL: **Dependence of giant magnetoresistance on oxygen stoichiometry and magnetization in polycrystalline $La_{0.67}Ba_{0.33}MnO_z$.** *Phys Rev B* 1995, **51:**6143–6146.
17. Moreno C, Abellan P, Sandiumenge F, Casanove MJ, Obradors X: **Nanocomposite lanthanum strontium manganite thin films formed by using a chemical solution deposition.** *Appl Phys Lett* 2012, **100:**023103–023106.
18. Sahu DR, Mishra DK, Huang JL, Roul BK: **Annealing effect on the properties of $La_{0.7}Sr_{0.3}MnO_3$ thin film grown on Si substrates by DC sputtering.** *Physica B* 2007, **396:**75–80.
19. Zhang N, Ding W, Zhong W, Xing D, Du Y: **Tunnel-type giant magnetoresistance in the granular perovskite $La_{0.85}Sr_{0.15}MnO_3$.** *Phys Rev B* 1997, **56:**8138–8142.
20. Li M, Wang GC: **Effect of surface roughness on magnetic properties of Co films on plasma-etched Si (100) substrates.** *J Appl Phys* 1998, **83:**5313–5321.

doi:10.1186/1556-276X-8-345
Cite this article as: Liang *et al.*: Nanoscale crystal imperfection-induced characterization changes of manganite nanolayers with various crystallographic textures. *Nanoscale Research Letters* 2013 **8**:345.